

Supplemental Information

Trans-omics Impact of Thymoproteasome in Cortical Thymic Epithelial Cells

Izumi Ohigashi, Yu Tanaka, Kenta Kondo, Sayumi Fujimori, Hiroyuki Kondo, Amy C. Palin, Victoria Hoffmann, Mina Kozai, Yosuke Matsushita, Shinsuke Uda, Ryo Motosugi, Jun Hamazaki, Hiroyuki Kubota, Shigeo Murata, Keiji Tanaka, Toyomasa Katagiri, Hidetaka Kosako, and Yousuke Takahama

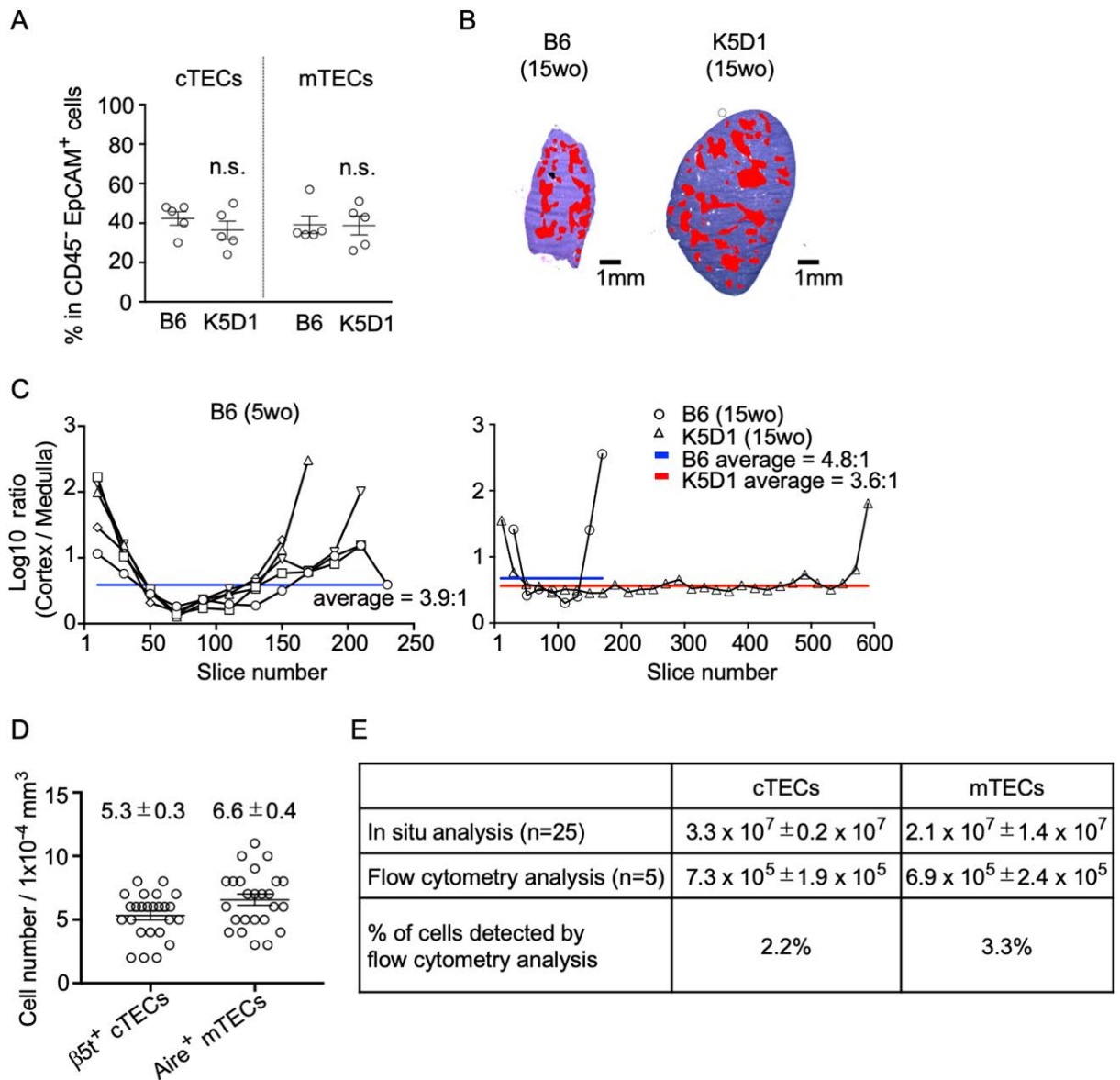


Figure S1. Distribution and recovery of TECs from K5D1 mice (Related to Figure 1)

(A) Flow cytometric analysis of TECs from B6 and K5D1 mice. Shown are plots of the frequency (means and SEMs, n = 5) of Ly51⁺ UEA1⁻ cTECs and Ly51⁻ UEA1⁺ mTECs within CD45⁺ EpCAM⁺ cells in B6 and K5D1 mice.

(B) Representative images of thymic sections stained with hematoxylin and eosin. Indicated mice were analyzed at 15 weeks old. Bar, 1 mm. The medullary regions were highlighted in red.

(C) Ratios (in logarithmic scale) of the cortex and the medulla in serial coronal sections of snap-frozen right-side thymic lobes obtained from 5-week-old B6 mice (left; Sakata, et al. 2018) and from 15-week-old B6 and K5D1 mice (right), according to the methods described previously (Sakata, et al. 2018). Blue and red lines represent the average ratios in B6 thymus (blue) and K5D1 mice (red).

(D) Numbers of $\beta 5t^+$ cTECs and Aire⁺ mTECs within a unit volume in the thymus of 15-week-old K5D1 mice were calculated as previously described (Sakata, et al. 2018). Means and SEMs of the numbers from 25 images are shown.

(E) Numbers of cTECs and mTECs in 15-week-old K5D1 mice were deduced from *in situ* thymic section analysis and flow cytometric analysis. The frequency of cells detected by flow cytometric analysis (i.e., numbers isolated from flow cytometric analysis / numbers deduced from *in situ* thymic section analysis) demonstrates equivalent efficiency of TEC isolation between 15-week-old K5D1 mice and 5-week-old B6 mice (Sakata, et al. 2018).

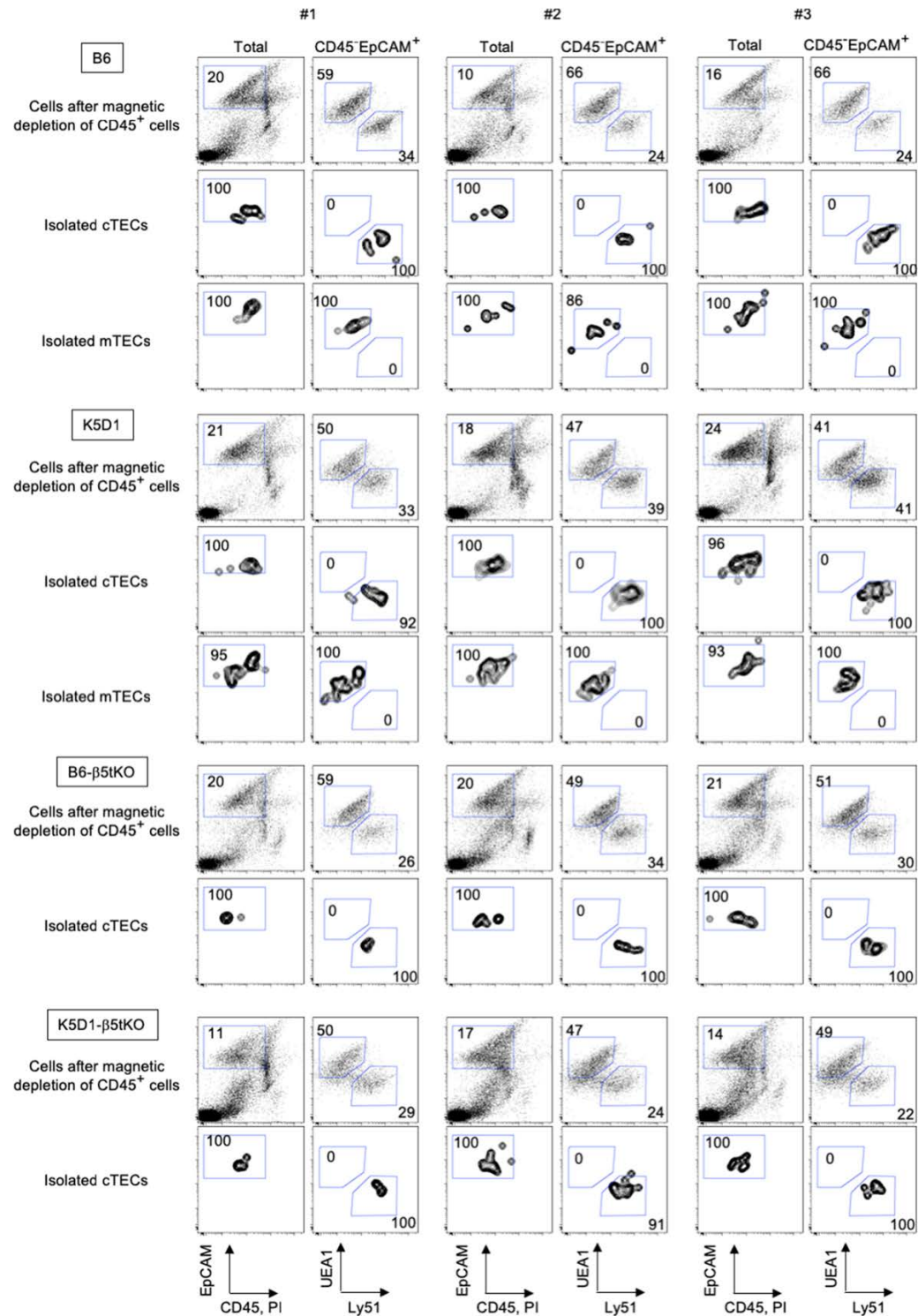


Figure S2. Purity of isolated cTECs and mTECs for transcriptomic and proteomic analyses
(Related to Figure 2)

Flow cytometric analysis of indicated cells (n = 3) from indicated mice. Numbers indicate frequency of cells within indicated areas.

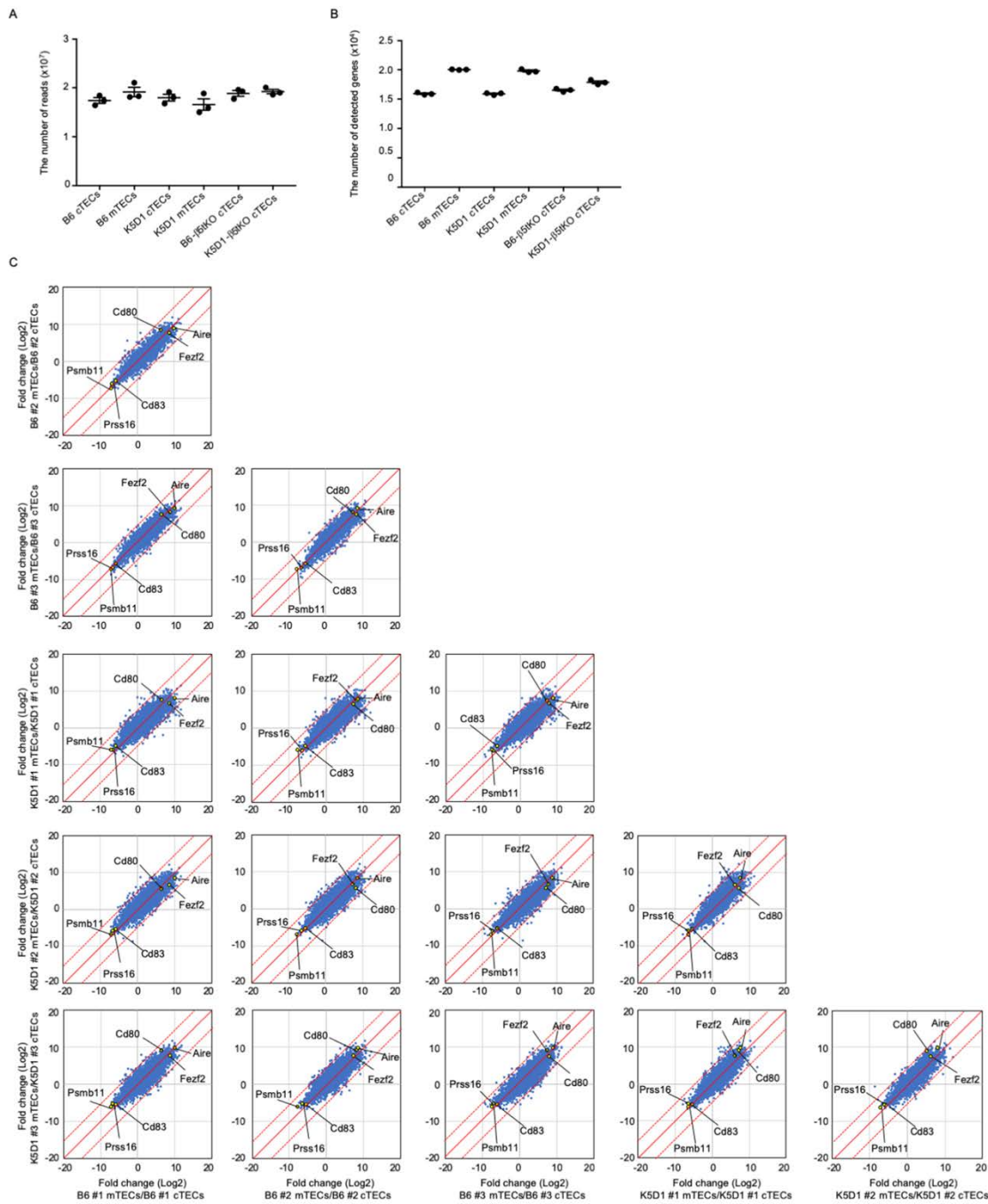


Figure S3. Numerical depths and unbiased comparisons of gene expression profiles for RNA sequencing analysis of K5D1 TECs and B6 TECs (Related to Figure 3)
(A) Number of reads (means and SEM, $n = 3$) and **(B)** number of detected genes in indicated cell populations.
(C) Correlation plot analysis of the transcriptome according to \log_2 fold change (mTECs / cTECs) among individual preparations.

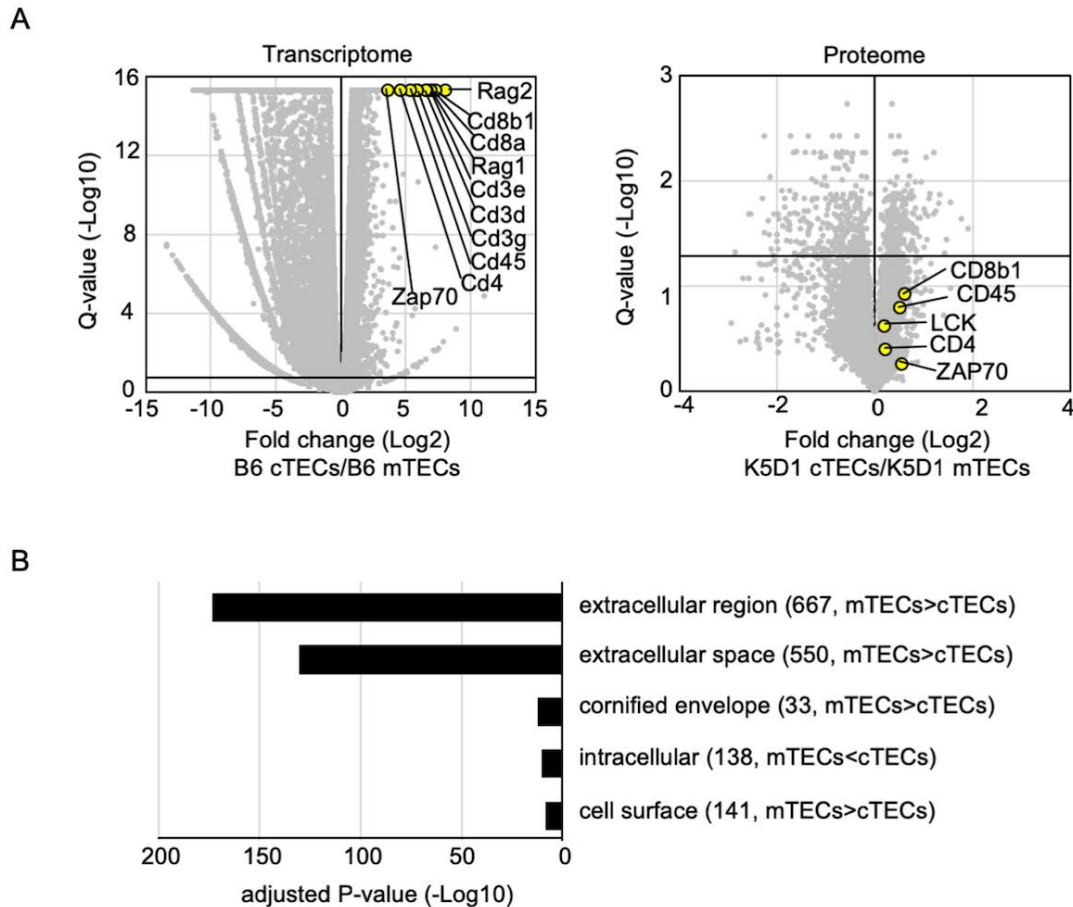


Figure S4. Trans-omics analysis of cTECs and mTECs (Related to Figure 4)

(A) Distinct contributions of TNC-enclosed CD4⁺CD8⁺ thymocytes in transcriptomic and proteomic analyses. Volcano plots of CD4⁺CD8⁺ thymocyte-derived molecules (yellow symbols) in RNA sequencing transcriptomic analysis (left) and TMT-based proteomic analysis (right). Detected molecules are plotted as log₂ fold changes (K5D1 cTECs / K5D1 mTECs) versus -log₁₀ Q-values. Black horizontal line in the plot shows the Q-value of 0.05.

(B) Enrichment analysis of the ontology for molecules differently expressed between mTECs and cTECs in transcriptomic analysis but not proteomic analysis. Molecules that were significantly different (RPKM > 1, log₂ fold change > 1 or < -1, Q < 0.05) between K5D1 mTECs and K5D1 cTECs in the transcriptomic analysis, annotated with the gene ontology, and not detected in the proteomic analysis (2,989 molecules for mTECs and 1,070 molecules for cTECs) were analyzed for the enrichment in the ontology. Bars show the adjusted P-value of top 5 categories enriched in either mTECs or cTECs. Numbers in parentheses indicate the number of categorized genes.

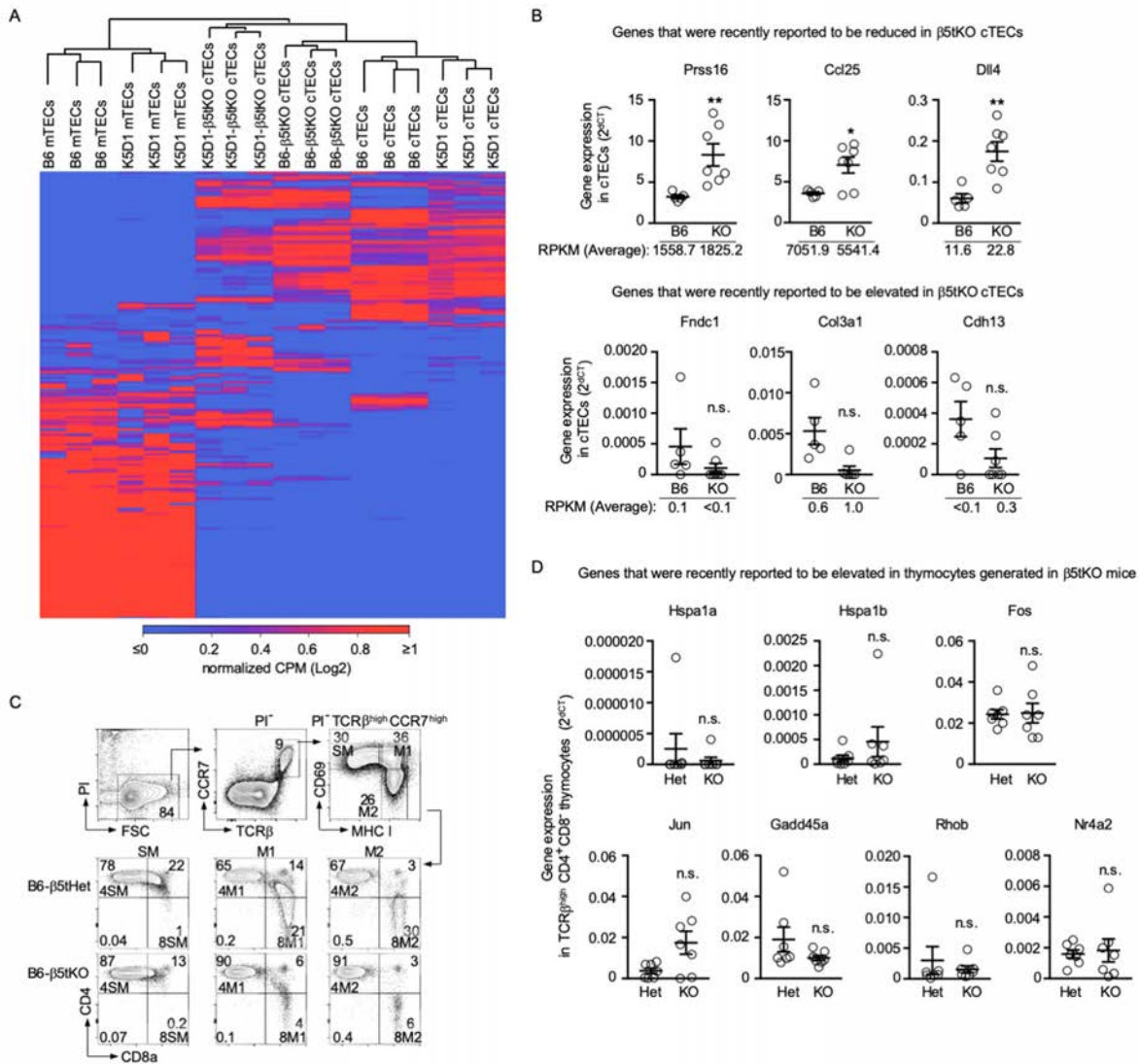


Figure S5. Transcriptomic analysis of cTECs and thymocytes in β 5t-KO mice (Related to Figure 5)

(A) Unsupervised hierarchical cluster analysis and heatmap of detected genes in indicated cTECs and mTECs ($n = 3$) isolated from B6 mice, K5D1 mice, B6- β 5tKO mice, and K5D1- β 5tKO mice.

(B) Quantitative RT-PCR analysis of the gene expression that was recently reported (Apavaloaei, et al., 2019) to be either reduced (top) or elevated (bottom) in β 5tKO cTECs in comparison with control cTECs. Plotted are the mRNA expression levels (means and SEMs, $n = 5-7$) of indicated genes relative to *Gapdh* in B6 cTECs and B6- β 5tKO cTECs. Numbers at the bottom of the plots show average RPKM values in RNA sequencing data.

(C) Shown are representative plots of propidium iodide (PI) fluorescence and forward scatter (FSC) intensity in total thymocytes (top left), CCR7 and TCR β expression in PI⁺ viable thymocytes (top middle), and CD69 and MHC class I expression in PI⁺ TCR β ^{high} CCR7^{high} viable thymocytes (top right). Plots in the middle and bottom panels show CD4 and CD8 α expression profiles in MHC class I^{low} CD69^{high} TCR β ^{high} CCR7^{high} semi-mature stage (SM) thymocytes (left), MHC class I^{high} CD69^{high} TCR β ^{high} CCR7^{high} mature 1 stage (M1) thymocytes (center), and MHC class I^{high} CD69^{low} TCR β ^{high} CCR7^{high} mature 2 stage (M2) thymocytes (right) in B6- β 5tHet mice (middle panels) and B6- β 5tKO mice (bottom panels). Numbers indicate frequency of cells within indicated areas.

(D) Quantitative RT-PCR analysis of gene expression that was recently reported (Apavaloaei, et al., 2019) to be elevated in TCR β ^{high} CD4⁺ CD8⁻ thymocytes in β 5tKO mice. Plotted are the mRNA expression levels (means and SEMs, $n = 7$) of indicated genes relative to *Gapdh* in TCR β ^{high} CD4⁺ CD8⁻ thymocytes isolated from B6- β 5tHet and B6- β 5tKO mice. * $P < 0.05$; ** $P < 0.01$; n.s., not significant.

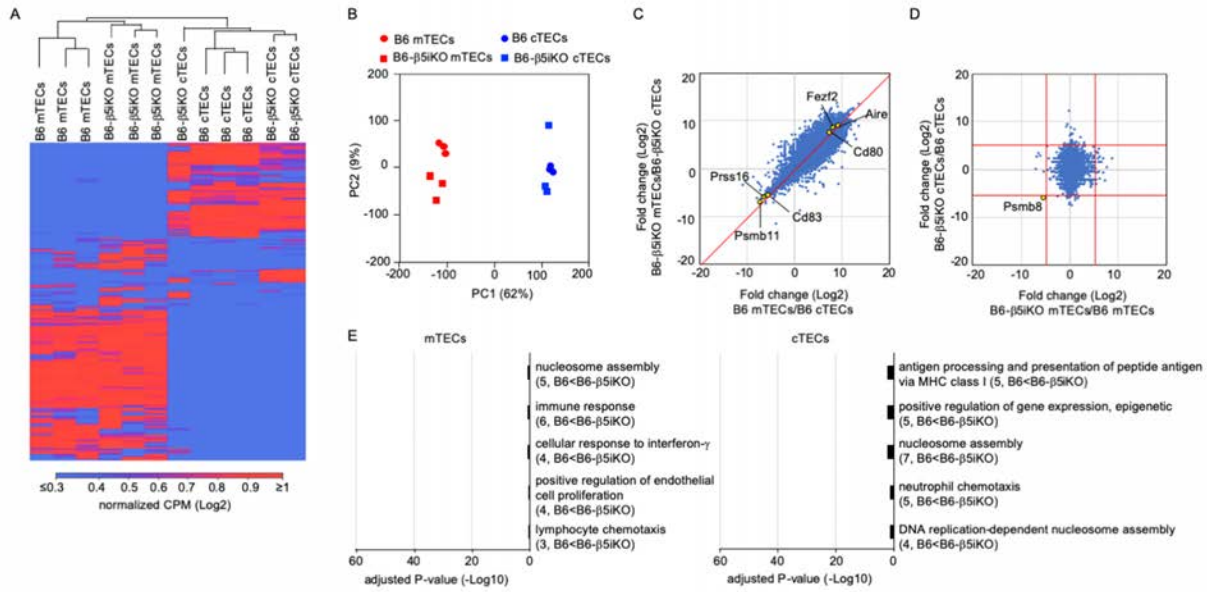


Figure S6. RNA sequencing analysis of cTECs and mTECs isolated from $\beta 5i$ -deficient mice

(Related to Figure 5)

(A) Unsupervised hierarchical cluster analysis and heatmap of genes detected in individual TEC samples ($n = 3$) isolated from B6 mice and B6- $\beta 5iKO$ mice.

(B) Principal component (PC) analysis of RNA sequencing data of indicated cell populations.

(C) Correlation plot analysis of the transcriptome according to \log_2 fold change (mTECs/cTECs) between B6 and B6- $\beta 5iKO$ TECs.

(D) Correlation plot analysis of the transcriptome according to \log_2 fold change (B6- $\beta 5iKO$ /B6) between mTECs and cTECs.

(E) Ontology enrichment analysis of genes that are differentially expressed ($RPKM > 1$, \log_2 fold change > 1 or < -1 , $Q < 0.05$) between B6 and B6- $\beta 5iKO$ TECs. Bars show the adjusted P-values of top five categories enriched in mTECs (left) and cTECs (right). Numbers in parentheses indicate the number of categorized genes.

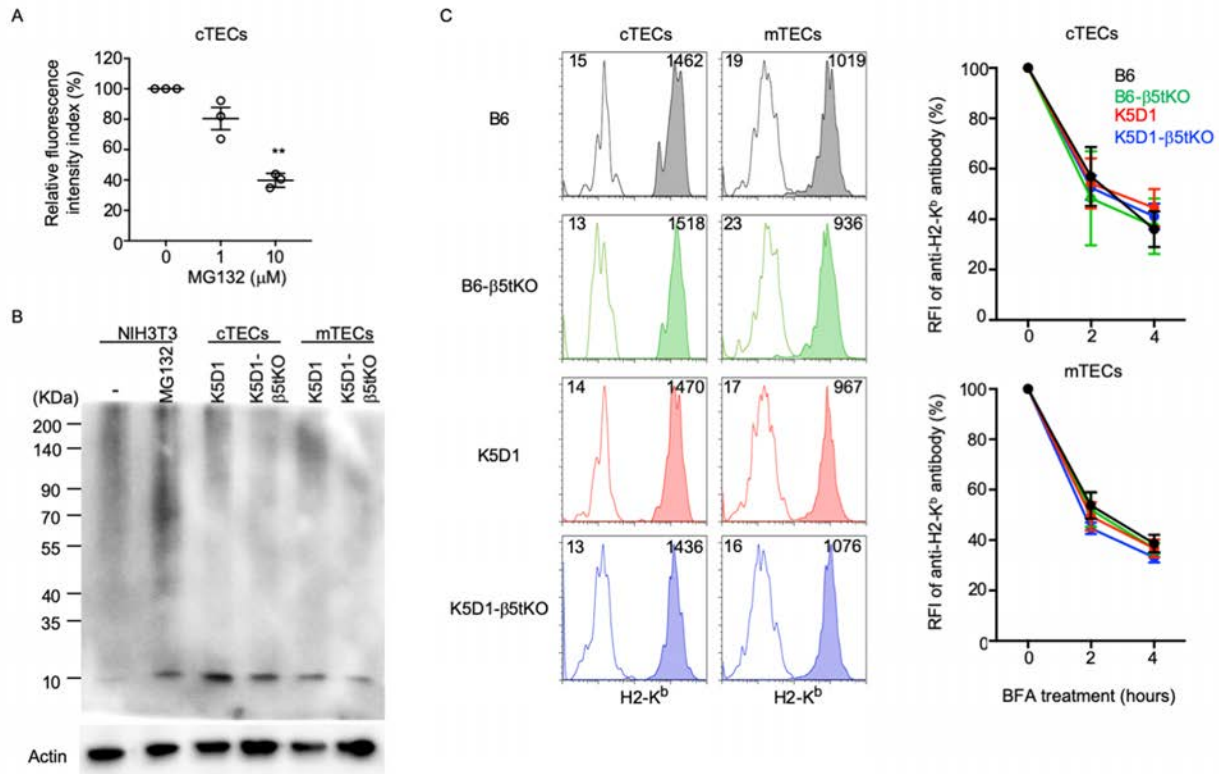


Figure S7. Characterization of cTECs and mTECs in β5t -deficient mice
(Related to Figure 7)

(A) Fluorescence-based proteasome activity in B6 cTECs in the presence of MG132 proteasome inhibitor. Shown are plots of relative fluorescence intensity index (means and SEMs, $n = 3$). $**P < 0.01$.

(B) Immunoblot analysis of ubiquitin in cTECs and mTECs isolated from K5D1 and K5D1- β5tKO mice. NIH3T3 cells with or without proteasome inhibitor MG132 treatment were also examined. Immunoblot for β -actin was examined as loading control.

(C) Cell surface expression and decay of MHC class I molecule H-2K^b expressed by cTECs and mTECs. Shaded histograms show H-2K^b expression on cTECs and mTECs in indicated mice, without brefeldin A treatment. Open histograms represent control fluorescence in the absence of anti-H-2K^b antibody. Numbers in histograms show the mean fluorescence intensities (MFIs) of isotype control antibody (left) and anti-H-2K^b antibody (right). Plots on the right show relative fluorescence intensity index (RFI, means and SEMs, $n = 4-7$) of H-2K^b expression at 2 and 4 hours after brefeldin A treatment in comparison with the intensity before the treatment.